Research Article

Journal of PeptideScience

Received: 20 December 2011 Revised: 27 March 2012 Accepted: 1 April 2012 Published online in Wiley Online Library: 21 May 2012

(wileyonlinelibrary.com) DOI 10.1002/psc.2415

Structural insights into the transmembrane domains of human copper transporter 1

Lei Yang, Zhaowei Huang and Fei Li*

The human copper transporter 1 (hCtr1) mediates cellular uptake of copper and Pt-based chemotherapeutic anticancer drugs. In this paper, we determined the three-dimensional structure and oligomerization of the transmembrane domains (TMDs) of hCtr1 in 40% HFIP aqueous solution by using solution-state NMR spectroscopy. We firstly revealed that TMD1 forms an α-helical structure from Gly67 to Glu84 and is dimerized by close packing of its C-terminal helix; TMD2 forms an α-helical structure from Leu134 to Thr155 and is self-associated as a trimer by the hydrophobic contact of TMD2 monomers; TMD3 adopts a discontinuous helix structure, known as 'α-helix-coiled segment-α-helix', and is dimerized by the interaction between the N-terminal helices. The motif GxxxG in TMD3 is not fully involved in the helix, but partially unstructured as a linker between helices. The flexible linker of TMD3 may serve as a gating adapter to mediate pore on and off switch. The differences in the structure and aggregation of the TMD peptides may be related to their different roles in the channel formation and transport function.

Supporting information can be found in the online version of this article.

Keywords: hCtr1 TMDs; structure; oligomerization; NMR

Introduction

Trace metal copper plays a crucial role in cells as a cofactor for many enzymes [1]. And it is important for cells to develop sophisticated homeostatic mechanisms to control intracellular copper accumulation and distribution [2,3]. At the protein level, two families of membrane proteins control cellular copper uptake and secretion: copper efflux is governed by the ATP-dependent pumps ATP7A and ATP7B [4,5], whereas copper influx is mediated by the copper transporter (Ctr) proteins.

The genes encoding high-affinity copper ion transport proteins were first indentified in the plasma membrane by studies in yeast cells [6]. The human high-affinity copper transporter (hCtr1) was subsequently isolated by the functional complementation of Ctr1-deficient yeast [7]. The hCtr1 has structural and functional similarities to the copper transporters in yeast [8]. Recent studies have provided the first insights into structure–function relationships of hCtr1 [9–11]. These studies suggested that hCtr1 constructs the copper trafficking pathway in biological membrane by a homotrimer. The second transmembrane helix is the key element lining the central pore of the structure, and the first and third transmembrane helices are involved in tight helix packing.

Recently, much more attentions have been concentrated on Ctr proteins, in part because Ctr proteins were linked to the cellular uptake of Pt-based chemotherapeutic anticancer drugs such as cisplatin [12–14]. Although significant progress has been made in characterizing the trafficking of copper and Pt-containing drugs, many of the structural properties and functional mechanisms of Ctr proteins have remained obscure because of lack of high-resolution structural information on the atomic level.

In the present work, we firstly determined the high-resolution structures of three hCtr1 fragments corresponding to transmembrane domain (TMD) 1, 2, and 3 of the protein and their aggregation in HFIP aqueous solution using solution-state NMR. We demonstrated the differences in the structure and aggregation of the peptides, which may be related to the different roles of them in the channel formation and transport function.

Materials and Methods

Materials

The peptides with the sequences of KNTAGEMAGAFVAVFLLAMFYEGLK, KHLLQTVLHIIQVVISYFLMLIFMTYNKK and YNGYLCIAVAAGAGTGYFLFSWKK, corresponding to transmembrane domain 1–3 (TMD1–TMD3) of hCtr1 (hCtr1 64–87, 132–157, and 156–179), respectively, were synthesized and purified by Shanghai Apeptide Co., Ltd (Shanghai, China). In order to increase the solubility of the peptides in purification, one Lys was added in the N-terminus of TMD1, one Lys in the N-terminus of TMD2, and two Lys in the C-terminus of TMD2 (underlined residues in the sequences). The purity was assessed by HPLC and mass spectroscopy. It was higher than 95%. The organic solvent 1,1,1,3,3,3-hexafluoro-2-propanol-d_2 (HFIP-d_2, 98%) was obtained from Cambridge Isotope Laboratories, Inc. (Andover, MA, USA), and HFIP (99.5%) was purchased from Acros Organics (Morris Plains, NJ, USA). The detergent dodecylphosphocholine (DPC, 99%) and sodium dodecyl sulfate (SDS, 99%) were obtained from Sigma-Aldrich (St. Louis, Missouri, USA). The

* *Correspondence to: Fei Li, State Key Laboratory of Supramolecular Structure and Materials, Jilin University, 2699 Qianjin Avenue, Changchun 130012, China. E-mail: feili@jlu.edu.cn*

State Key Laboratory of Supramolecular Structure and Materials, Jilin University, 2699 Qianjin Avenue, Changchun 130012, China

phospholipids 1-palmitoyl-2-oleoyl-sn-glycero-3-phosphocholine (POPC) was purchased from Avanti Polar Lipids Inc (Alabaster, Alabama, USA). All chemicals were used directly after purchase without further purification.

Sample Preparation

The samples of 2 mM peptides in 40% HFIP-d_2 aqueous solution used in the NMR experiments were prepared by solvating appropriate amount of peptides in 200 μl pure HFIP-d_2 solvent and then adding deionized water to a total volume of 500 μl.

The samples used in the CD experiments were 20 μM peptides in 40% HFIP aqueous solution, 20 μM peptides in 10 mM DPC or SDS surfactant, or in 3 mM POPC lipid. The samples of peptides in 40% HFIP aqueous solution were prepared using similar approach as described in the NMR sample preparation. The POPC lipid samples were prepared according to the following method. Briefly, the peptide powder was dissolved in HFIP solvent to prepare a stock solution, and the POPC powder was dissolved in the chloroform/methanol (2 : 1 v/v) co-solvent. An appropriate amount of peptide stock solution was mixed with the chloroform/methanol (2 : 1 v/v) co-solvent of POPC to obtain the molar ratio of peptide : lipid to 1 : 150. The mixture was dried under a nitrogen stream. The obtained lipid film was kept under vacuum overnight to remove residual organic solvents. The dried lipid film was hydrated using deionized water. Finally, the lipid suspension was sonicated for at least 60 min in the bath-type sonicator at 40 °C. The pH of the solution was 6.8. The DPC and SDS micellar samples of the peptides were prepared by mixing 200 μl HFIP solution of peptide (stock solution) with 200 μl detergent aqueous solution according to the molar ratio of peptide : detergent 1 : 500 and then diluting the mixture further with deionized water to 1 : 16 (v/v) of HFIP : water. After lyophilization overnight, the resulting dry powder was rehydrated with deionized water. The corresponding blank samples without peptides were also prepared using the same methods.

For the preparation of the samples of the SDS-PAGE experiments, equal amounts of peptide/HFIP stock solutions with the same peptide concentration were added in separate tubes and dried with nitrogen flow. After adding equal volumes of loading buffer [100 mM Tris-Cl at pH 6.8, 8% (w/v) SDS, 0.2% (w/v) bromophenol blue, 24% (v/v) glycerol] and dithiothreitol [15,16], the mixtures were boiled for 30 min prior to loading. The running buffer contained 100 mM Tris, 100 mM tricine, and 0.1% (w/v) SDS.

NMR Experiments

NMR experiments were performed on a Bruker Avance 500-MHz spectrometer at 298 K. A 5-mm triple resonance inverse probe with z-gradient coil was used. The TOCSY spectra were recorded with mixing time of 100 ms. The NOESY spectra were recorded with mixing times 50, 100, 150, and 200 ms, and all structures were calculated using the data from the NOESY spectrum with mixing time of 200 ms. The WATERGATE technique was used in both experiments for water suppression [17]. Standard Bruker software (XWINNMR Version 3.5) and Sparky suit [18] of programs were used for spectra processing, visualization, and peak picking. Standard procedures based on spin-system identification and sequential assignment were adopted to identify the resonances [19]. The proton chemical shifts were referenced to TSP [sodium salt of 3-(trimethylsilyl)-propionate-2,2,3,3-d_4] in the sample. The chemical shifts and NOE intensities served as input files for the structural calculation were extracted from the TOCSY and NOESY spectra using SPARKY software.

Diffusion ordered spectroscopy (DOSY) spectra for the diffusion coefficient measurements of the peptides were recorded, and the apparent molecular weights were estimated using previous method [20]. In this work, 0.891×10^{-3} N s m^{-2} was used for the viscosity of pure H_2O to calculate the viscosity of the 40% HFIP-d_2 aqueous solution containing peptide [21], 6.99×10^{-4} m^3 kg^{-1} was used for the partial specific volume of solvent molecule (v_1) [22], and the partial volumes of peptides (v_2) were 7.54×10^{-4} m^3 kg^{-1} for TMD1, 7.80×10^{-4} m^3 kg^{-1} for TMD2, and 7.39×10^{-4} m^3 kg^{-1} for TMD3, which were calculated according to the method of the reference [23].

Structure Calculation

The structural calculations were performed using the program CYANA (version 1.0.6) package [24]. The NOE intensities and chemical shifts were served as input data. The NOE intensities were transformed into the upper limits of the distance restraints using the CALIBA program. These distance restraints were subjected to a systematic analysis of the local conformation around the C_α atom of each residue, including the dihedral angles ϕ, ψ, χ^1, and χ^2, using the macro GRIDSEARCH. Torsion angle dynamic calculations were performed by the macro ANNEAL. The calculations were started from 200 initial random structures and structures with no violations >0.2 Å for distance restraints and $>5.0°$ for angle restraints were accepted. An ensemble of 20 structures with the lowest target functions were chosen for structural analysis using the PROCHECK-NMR program [25]. Visual analyses of the structures and figure drawings were achieved by the MOLMOL program [26].

Far-UV CD Measurements

Far-UV CD spectra were recorded on a Jasco J-810 spectropolarimeter with a continuous flow of nitrogen purging the polarimeter at room temperature. The prepared samples were added in a cylindrical cell with 0.5-mm path lengths. The CD experiments were carried out in a wavelength range between 190 and 260 nm with scan speed 50 nm/min, data pitch 0.1 nm, response time 0.25 s, and bandwidth 1 nm. The spectra were scanned three times for each sample and averaged, and the blank was subtracted from all spectra. Final spectra were smoothed using a FFT filter, and the intensity was expressed as mean residue ellipticity [27]. Secondary structure analysis was performed by CDPro software package [28].

SDS-PAGE

The electrophoresis was performed at room temperature. Samples were completely loaded into the separating gel using 30 V before increasing the voltage to 130–150 V for the electrophoresis. Equal amounts of peptide samples with the same concentration were loaded in each of the lanes. For sharpening the bands of peptides, a 10% 'spacer gel' was introduced between 4% stacking and 16.5% separating gels. The bands of peptides were visualized with Coomassie Brilliant Blue R-250 stain. The protein standards with ultra low molecular weight (3.5–26.6 kDa) were used to estimate the apparent molecular weights of the peptides studied.

Journal of PeptideScience

Results

The Secondary Structures of the Peptides in Various Membrane-Mimic Environments

The Far-UV CD spectra of the peptides TMD1–TMD3 in lipid vesicles (POPC), micelles (DPC and SDS), and 40% HFIP aqueous solution were measured to characterize the secondary structures of these peptides. As shown in Figure 1, the TMD1 and TMD2 display similar spectral character in all these environments, i.e., a positive band at ~194 nm and two negative bands at ~208 and ~222 nm, suggesting a typical α-helical structure for the peptides. The CD spectra of TMD3 in 40% HFIP aqueous solution and POPC lipid vesicle also display a helical type of absorbance but with a lower helicity, where the typical CD absorbance of helix could not be observed for TMD3 in micelles. Moreover, the order of helical length with TMD2 > TMD1 > TMD3 was observed in all these membrane mimics (see Table S1 in the supporting information).

Three-Dimensional Structures of the Peptides in 40% HFIP-d_2 Aqueous Solution

We measured the NMR spectra of the TMD peptides in 40% HFIP-d_2 aqueous solution at 298 K. The 2D NMR spectra of the peptides in 40% HFIP-d_2 aqueous solution showed dispersed cross peaks. The NMR resonance assignments of the three peptides in 40% HFIP-d_2 aqueous solution at 298 K are given in the supporting information (Table S2–S4).

In the NOESY spectrum of TMD1, a series of sequential NOE connectivities [Hα(i)-HN(i + 1), Hβ(i)-HN(i + 1), and HN(i)-HN(i + 1)] and medium-range connectivities [Hα(i)-HN(i + 3), Hα(i)-Hβ(i + 3), and Hα(i)-HN(i + 4)] from Thr3 to Gly23 were found (Figure 2), predicting the formation of an α-helical structure in this residue region. A total of 221 non-redundant distance constraints and 74 angle constraints resulting from 321 NOE cross peaks in the NOESY spectrum were used in the structure calculation. The 20 structures that have the lowest target function and neither distance violations larger than 0.2 Å nor dihedral angle violations larger than 5° were estimated using the Ramachandran analyses of main chain dihedral angles. A mean structure of the 20 structures displays an α-helix spanning from Gly5 to Glu22 in TMD1 (Gly67–Glu84 in hCtr1). The chemical shift index (CSI) [29] also displays similar structural characteristics in the same residue region. The final results obtained from the structural calculation are shown in Figure 3.

A long α-helix nearly from the N-terminal to the C-terminal end is implicated for TMD2 by a series of medium-range NOE connectivities from His2 to Asn27 (Figure 2). The structural calculation using a total of 329 non-redundant distance constraints and 101 angle constraints extracted from 503 NOE cross peaks assumes an α-helix spanning from Leu4 to Thr25 (Leu134–Thr155 in hCtr1), as shown in Figure 3. The helix is a little bent and displays an amphiphilic residue distribution with the polar residues in the same side and the other face occupied by non-polar residues. The residues His9, Ser16, Met20, and Met24 (His139, Ser146, Met150, and Met154 in hCtr1, respectively) that may be important for function [30] lie in the same face of the helix.

The TOCSY and NOESY spectra of TMD3 in 40% HFIP-d_2 aqueous solution were broadened severely and displayed two groups of cross peaks for the residues in the C-terminal part, such as Ala13, Gly14, Thr15, Gly16, Phe18, Leu19, Phe20, Lys23, and Lys24 (the second group of cross peaks of Lys23 and Lys24 only appeared in the TOCSY spectrum). The two groups of cross peaks have similar $\delta_{H\alpha}$ values but largely different δ_{HN} values, and one group of the cross peaks has much stronger intensities than the

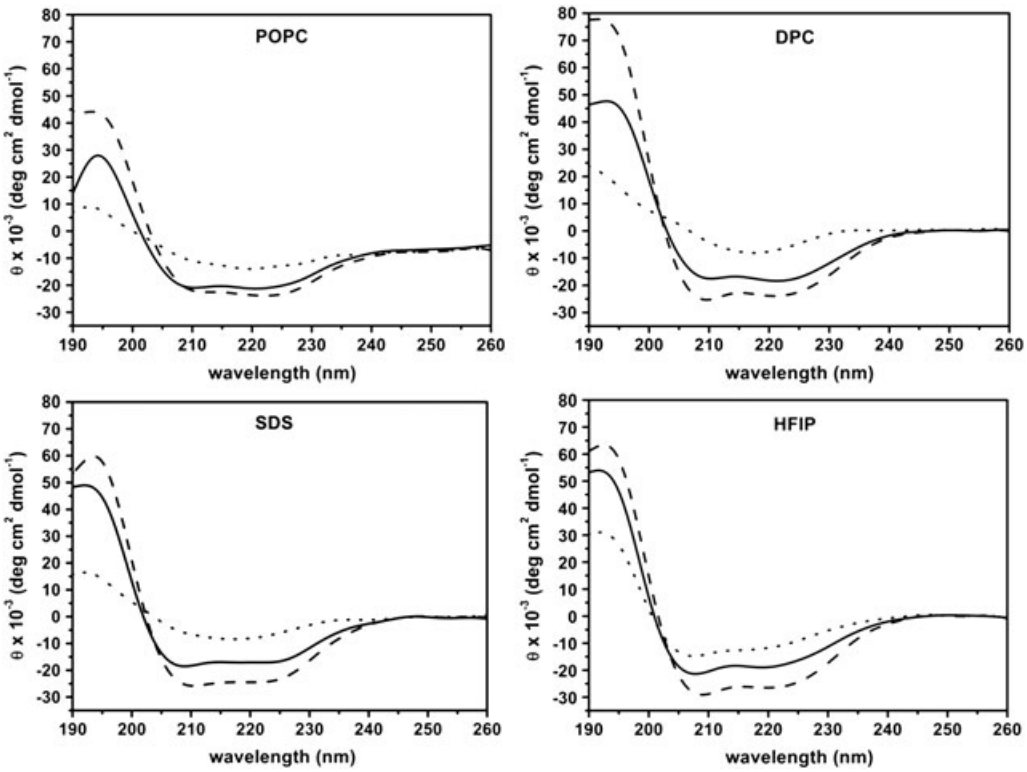

Figure 1. CD spectra of the transmembrane peptides TMD1 (solid), TMD2 (dashed), and TMD3 (dotted) in various membrane mimics at room temperature.

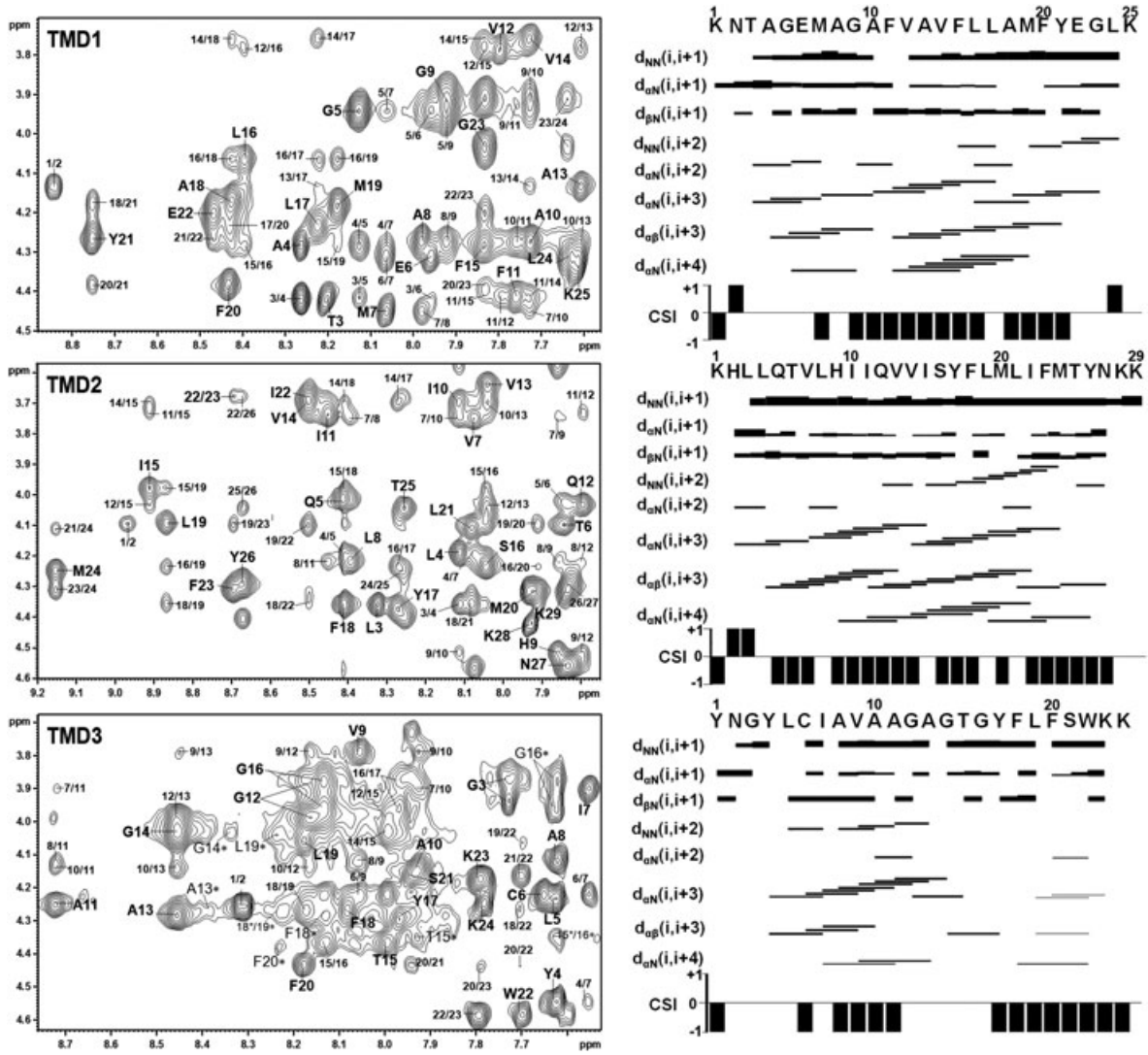

Figure 2. Hα-HN region of 2D NOESY spectra with assignments (left) and NOE connectivities along with the chemical shift index (right) for the peptides in 40% HFIP-d_2 aqueous solution at 298 K. Two groups of cross peaks are assigned in the NOESY spectrum of TMD3, where the secondary group of cross peaks are marked with asterisk.

other (Figure 2). We attributed the two groups of signals to different aggregate states of TMD3. We used the group of cross peaks with stronger intensities as the input data of CYANA calculation. Accordingly, 154 non-redundant distance limits and 68 angle constraints were used for structural calculations obtained from 255 NOE cross peaks. Most of the distance constraints of Hα(i)-HN (i + 3), Hα(i)-Hβ(i + 3), and Hα(i)-HN(i + 4) were found in the range of Tyr4–Thr15 and Phe18–Trp22 (Figure 2). As a result, two α-helical segments spanning from Cys6 to Gly14 and Phe18 to Ser21 in TMD3 were obtained (Figure 3). The region between helices is a coil or disordered structure. The CSI showed similar structural character with a continuous '0' value between Gly12 and Gly16 and a dense/continuous '−1' in the region of helices. The structural statistics of all TMDs in 40% HFIP aqueous solution at 298 K are summarized in Table S5 in the supporting information.

Oligomeric State of the Peptides

The oligomerization state of the three transmembrane peptides was probed by DOSY measurements. The three peptides demonstrated similar diffusivity in 40% HFIP aqueous solution (Figure S1 in the supporting information). The diffusion coefficients obtained from DOSY were 7.727×10^{-11} for TMD1, 6.678×10^{-11} for TMD2, and 7.668×10^{-11} for TMD3, corresponding to the apparent molecular weights of 4798, 9217, and 4546 Da, respectively. Therefore, trimerization of TMD2 and dimerization of TMD1 and TMD3 were suggested (the monomeric molecular weights of TMD1, TMD2, and TMD3 are 2679, 3535, and 2600 Da, respectively). As mentioned earlier, two groups of NMR signals were observed in the 2D NOESY and TOCSY spectra of TMD3 for the residues of its C-terminal part, and the intensities of one group of signals were much stronger than those of the other one. The diffusion coefficient obtained from the DOSY spectrum of TMD3 is attributed to that of the peptide component with stronger intensities of signals. The aggregate state of the peptide component with weaker intensities is unclear because this group of signals was not observed in the DOSY spectrum.

Of the proton chemical shifts of the peptide backbone, $\delta_{H\alpha}$ is correlated to the secondary structure of the peptide, whereas δ_{HN} is more sensitive to the environment where the peptide is involved in. It was found that the exposure of a peptide to a hydrophobic environment, such as the surface of HFIP cluster or inside of micelle, results in its δ_{HN} more upfield relative to that

Journal of PeptideScience

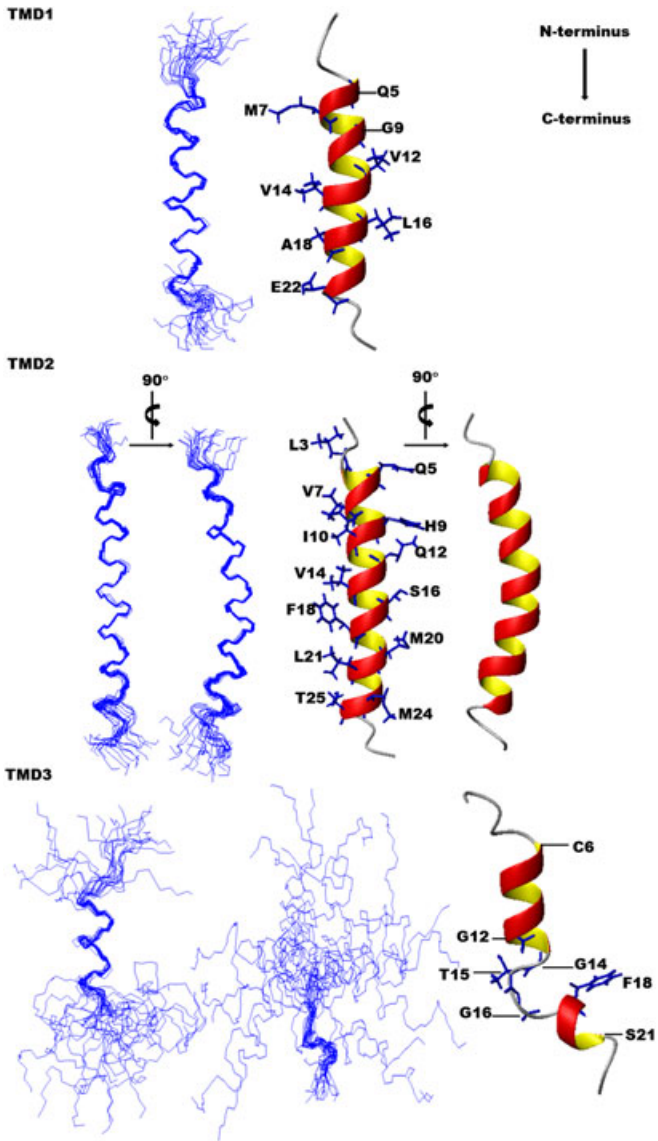

Figure 3. Structures of the peptides in 40% HFIP-d_2 aqueous solution: an ensemble of the 20 structures with the lowest target function presented as backbone atoms and a ribbon representation of the mean structure of the 20 structures. The 20 backbone structures were fitted over each helical region (see Table S5 in the supporting information).

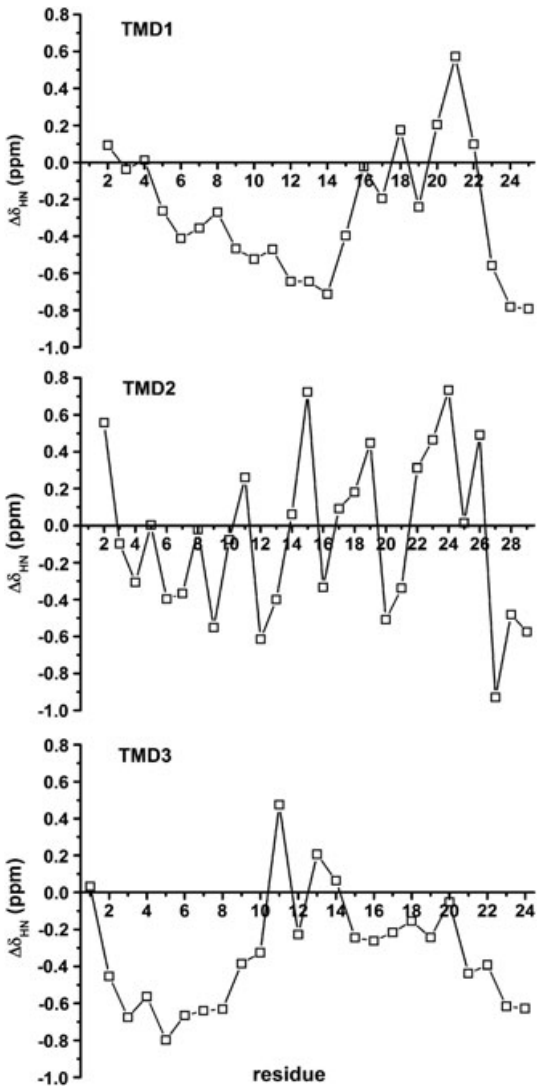

Figure 4. The differences in δ_{HN} of the peptides in 40% HFIP/60% H_2O relative to the peptide in water.

of the peptide with an unfolded conformation in aqueous medium. This is true for most of residues of the three peptides in 40% HFIP-d_2 aqueous solution. However, it is interesting to notice that the δ_{HN} values of some residues of the peptides are evidently downfield shifted in 40% HFIP-d_2 aqueous solution in comparison with their δ_{HN} values in water (Figure 4), such as Ala18 and Tyr21 of TMD1; Ala11 and Ala13 of TMD3; and His2, Ile11, Ile15, Phe18, Leu19, Ile22, Phe23, Met24, and Tyr26 of TMD2. The residues with a downfield shift of δ_{HN} were assigned to the residues that are involved in the intermolecular interactions, in which the HN protons of these residues may play a role by forming intermolecular hydrogen bonds. For TMD1 and TMD3, only a few residues with the downfield shift of δ_{HN} imply a small area of intermolecular contact and less association stability. In contrast, there are more residues with the downfield shift of δ_{HN} for TMD2, and they are mainly apolar residues in the region of Ile11–Met24 with an approximate i/i+3 or i/i+4 sequential alignment; whereas the δ_{HN} values of the N-terminal part of the helix are either less changed or upfield shifted. This means that TMD2 monomers may adopt a more parallel molecular orientation in the trimer through a larger area of residue contacts in the C-terminal part of helix, but allowing the N-terminal part of the helices more distant and more exposed to HFIP aqueous solution. A pore formation may be assumed for TMD2 in consideration of its trimeric aggregation. Detailed intermolecular interactions among residues are unclear because no unambiguous intermolecular NOEs were observed for the three TMD peptides.

The aggregation state of the three transmembrane peptides was further analyzed by SDS-PAGE, which is often used to probe qualitatively occurrence of transmembrane helix oligomerization [31,32]. The electrophoresis results of the peptides on the 16.5% polyacrylamide tris–tricine gel display a clearly visible band at a position corresponding to an apparent molecular weight of around 3 kDa for TMD1 and TMD3, but a smear band between the apparent molecular weights of ca. 4 and 7 kDa for TMD2 (Figure S2 in the supporting information), indicating a monomer state for either TMD1 or TMD3 and a coexistence of dimer and monomer for TMD2. Different from the results of the DOSY

measurements, the peptides are dissociated in the SDS-PAGE procedure. This may be attributed to unfolding effect of the detergent SDS to the peptide helices when heating samples, which may reduce the interaction between peptide monomers. Nevertheless, the SDS-PAGE results suggest that the second transmembrane domain of hCtr1 has intense propensity to aggregate than the first and third transmembrane domains.

Discussion

Because of the crucial role of the copper transporters in the uptake of cellular copper and platinum-based anticancer drugs, scientists are increasingly interested in the transport mechanisms of Ctr1 proteins. However, deep understanding to the function mechanisms is impeded largely by lack of high-resolution structural information on Ctr1 proteins. Because of difficulties in determining the structures of the integral membrane proteins, we studied in this paper the structure and oligomeric state of three isolated transmembrane domains (TMD1, TMD2, and TMD3) of hCtr1 in different membrane mimics. Because the structure determination of the TMD peptides in micelles by NMR technique was prevented by severe broadening of NMR signals (Figure S3 in the supporting information), we determined the structure of the TMD peptides in 40% HFIP aqueous solution using NMR. The results probed in HFIP aqueous solution should be comparable with those probed in POPC vesicles because the secondary structures of the peptides in HFIP aqueous solution are similar to those of the peptides in POPC lipid vesicles, as shown by the CD spectra. The functions of Ctr1 proteins are associated with their oligomerization; therefore, we also explored the oligomeric state of the peptides by DOSY and SDS-PAGE measurements.

Previous studies using cryo-electron microscopy technique has demonstrated that hCtr1 is trimerized in membrane, and the trimeric hCtr1 contains a cone-shaped pore; TMD2 is the principal pore lining helix of hCtr1 trimer, and the C-terminal end (with MxxxM motif) of each TMD2 subunit is closer than the N-terminal end of the transmembrane domain. In contrast, TMD1 and TMD3 in the hCtr1 trimer are in close contact through their middle regions [9,10]. Our NMR study reveals that TMD2 forms an amphiphilic α-helix spanning over Leu4 to Thr25 (Leu134–Thr155 in hCtr1) and aggregates as a trimer in 40% HFIP aqueous solution. The trimerization of TMD2 may be induced by the interactions of the apolar residues in the region from the center (Ile11) to the C-terminal end (Met24) of the helix; and the residues Ile11, Ile15, Leu19, and Met24 may be involved in a close contact between monomers, whereas the intermolecular interaction in the N-terminal part of TMD2 helices may be weaker, as indicated by the result of δ_{HN} shifting. If a pore is assumed for TMD2 trimer, the pore size at the C-terminal end (extracellular end of TMD2 in hCtr1) should be smaller than that of the N-terminal end (intracellular end of TMD2 in hCtr1). This is generally in agreement with the topology of hCtr1 pore obtained by cryo-electron microscopy technique [10]. This trimeric model may represent approximately one of the intermediate states of TMD2 in the transport process.

In the three transmembrane domains of hCtr1 transporter, the TMD2 constructs the inner wall of pore and participates in copper ion transfer directly. Therefore, the aggregate structure of TMD2 plays an important role in the biological function. Although the relative orientation and the relative distance of TMD2 monomers in the aggregate structure are influenced by the interactions with TMD1 and TMD3, the information of both detailed structure at atomic level and the intermolecular interactions of TMD2 might be obtained by the study of isolated peptide and will shed light on the structure of hCtr1 pore and mechanism of its function.

In the case of TMD1, an α-helix structure spanning over Gly5–Glu22 (Gly67–Glu84 in hCtr1) was determined by the NMR measurement. The helix can dimerize by the close contact of the residues in the C-terminal part of helices, which is suggested by evident downfield shifting of δ_{HN} of the residues Ala18 and Tyr21. However, an 'α-helix-coiled segment-α-helix' structure, but not a continuous helix as assumed previously, was unexpectedly obtained for TMD3. Part of the motif G12xxxG16 (such as Thr15 and Gly16) is not involved in helix, but in the flexible linker region. Evident downfield shift of δ_{HN} of Ala11 and Ala13 suggests that these residues are involved in the close intermolecular contact in the dimer. We guess that the complementary size of TMD1 and TMD3 in the middle region (two Val, two Leu, and two Phe in TMD1; three Gly and three Ala in TMD3) and possibly electrostatic interaction between Glu22 of TMD1 and Lys23 of TMD3 in the C-terminal ends may cause tight packing of the two domains in the same protein subunit.

The α-helix-coiled segment-α-helix conformation in TMD3 may be also important for the cooperative dynamics of TMD2 and TMD3 in the opening/closing state transfer of hCtr1 channel. The change in the size of channel entrance may be regulated by the relative orientation of TMD2 helices lining the inner of the channel, which could induce a cooperative change in the orientation of TMD3 helices because the loop between TMD2 and TMD3 is very short (only three residues). The flexible linker between the helices of TMD3 accommodates a partial change of the N-terminal half helix in the orientation. This means that the central flexible region in TMD3 may serve as a gating adapter to mediate the ionic channel on and off.

Acknowledgement

This work was financially supported by the NSFC (20973083 and 20934002).

Supporting Information

Supporting information may be found in the online version of this article.

References

1 Puig S, Thiele DJ. Molecular mechanisms of copper uptake and distribution. *Curr. Opin. Chem. Biol.* 2002; **6**: 171–180.
2 Askwith C, Kaplan J. Iron and copper transport in yeast and its relevance to human disease. *Trends Biochem. Sci.* 1998; **23**: 135–138.
3 Pena MM, Lee J, Thiele DJ. A delicate balance: homeostatic control of copper uptake and distribution. *J. Nutr.* 1999; **129**: 1251–1260.
4 Voskoboinik I, Camakaris J. Menkes copper-translocating P-type ATPase (ATP7A): biochemical and cell biology properties, and role in Menkes disease. *J. Bioenerg. Biomembr.* 2002; **34**: 363–371.
5 Lutsenko S, Efremov RG, Tsivkovskii R, Walker JM. Human copper-transporting ATPase ATP7B (the Wilson's disease protein): biochemical properties and regulation. *J. Bioenerg. Biomembr.* 2002; **34**: 351–362.
6 Knight SA, Labbe S, Kwon LF, Kosman DJ, Thiele DJ. A widespread transposable element masks expression of a yeast copper transport gene. *Genes Dev.* 1996; **10**: 1917–1929.
7 Zhou B, Gitschier J. hCTR1: a human gene for copper uptake identified by complementation in yeast. *Proc. Natl. Acad. Sci. U. S. A.* 1997; **94**: 7481–7486.

8 Lee J, Pena MM, Nose Y, Thiele DJ. Biochemical characterization of the human copper transporter Ctr1. *J. Biol. Chem.* 2002; **277**: 4380–4387.
9 Aller SG, Unger VM. Projection structure of the human copper transporter CTR1 at 6-A resolution reveals a compact trimer with a novel channel-like architecture. *Proc. Natl. Acad. Sci. U. S. A.* 2006; **103**: 3627–3632.
10 De Feo CJ, Aller SG, Siluvai GS, Blackburn NJ, Unger VM. Three-dimensional structure of the human copper transporter hCTR1. *Proc. Natl. Acad. Sci. U. S. A.* 2009; **106**: 4237–4242.
11 Schushan M, Barkan Y, Haliloglu T, Ben-Tal N. C(alpha)-trace model of the transmembrane domain of human copper transporter 1, motion and functional implications. *Proc. Natl. Acad. Sci. U. S. A.* 2010; **107**: 10908–10913.
12 Komatsu M, Sumizawa T, Mutoh M, Chen ZS, Terada K, Furukawa T, Yang XL, Gao H, Miura N, Sugiyama T, Akiyama S. Copper-transporting P-type adenosine triphosphatase (ATP7B) is associated with cisplatin resistance. *Cancer Res.* 2000; **60**: 1312–1316.
13 Ishida S, Lee J, Thiele DJ, Herskowitz I. Uptake of the anticancer drug cisplatin mediated by the copper transporter Ctr1 in yeast and mammals. *P Natl Acad Sci USA.* 2002; **99**: 14298–14302.
14 Kuo M, Chen H, Song I-S, Savaraj N, Ishikawa T. The roles of copper transporters in cisplatin resistance. *Cancer Metastasis Rev.* 2007; **26**: 71–83.
15 Schagger H, von Jagow G. Tricine-sodium dodecyl sulfate–polyacrylamide gel electrophoresis for the separation of proteins in the range from 1 to 100 kDa. *Anal. Biochem.* 1987; **166**: 368–379.
16 Schagger H. Tricine-SDS-PAGE. *Nat. Protocols.* 2006; **1**: 16–22.
17 Liu M, Mao X-A, Ye C, Huang H, Nicholson JK, Lindon JC. Improved WATERGATE pulse sequences for solvent suppression in NMR spectroscopy. *J. Magn. Reson.* 1998; **132**: 125–129.
18 Goddard TD, Kneller DG. *SPARKY 3*. University of California: San Francisco, CA, 2001.
19 Wüthrich K. *NMR of Proteins and Nucleic Acids*. Wiley: New York, 1986.
20 Xiao SY, Wang YX, Yang L, Qi HY, Wang CY, Li F. Study on structure and assembly of the third transmembrane domain of Slc11a1. *J. Pept. Sci.* 2010; **16**: 249–255.
21 Cho CH, Urquidi J, Singh S, Robinson GW. Thermal offset viscosities of liquid H_2O, D_2O, and T_2O. *J. Phys. Chem. B* 1999; **103**: 1991–1994.
22 Fioroni M, Burger K, Mark AE, Roccatano D. Model of 1,1,1,3,3,3-hexafluoro-propan-2-ol for molecular dynamics simulations. *J. Phys. Chem. B* 2001; **105**: 10967–10975.
23 Perkins SJ. Protein volumes and hydration effects. The calculations of partial specific volumes, neutron scattering matchpoints and 280-nm absorption coefficients for proteins and glycoproteins from amino acid sequences. *Eur. J. Biochem.* 1986; **157**: 169–180.
24 Guntert P, Mumenthaler C, Wuthrich K. Torsion angle dynamics for NMR structure calculation with the new program DYANA. *J. Mol. Biol.* 1997; **273**: 283–298.
25 Laskowski RA, Rullmannn JA, MacArthur MW, Kaptein R, Thornton JM. AQUA and PROCHECK-NMR: programs for checking the quality of protein structures solved by NMR. *J. Biomol. NMR* 1996; **8**: 477–486.
26 Koradi R, Billeter M, Wuthrich K. MOLMOL: a program for display and analysis of macromolecular structures. *J. Mol. Graph.* 1996; **14**: 51–55, 29–32.
27 Qi HY, Yang L, Xue R, Song YD, Wang S, Li F. The third and fourth transmembrane domains of Slc11a1: comparison of their structures and positioning in phospholipid model membranes. *Biopolymers* 2009; **92**: 52–64.
28 Sreerama N, Woody RW. Estimation of protein secondary structure from circular dichroism spectra: comparison of CONTIN, SELCON, and CDSSTR methods with an expanded reference set. *Anal. Biochem.* 2000; **287**: 252–260.
29 Wishart DS, Sykes BD, Richards FM. The chemical shift index: a fast and simple method for the assignment of protein secondary structure through NMR spectroscopy. *Biochemistry* 1992; **31**: 1647–1651.
30 De Feo CJ, Mootien S, Unger VM. Tryptophan scanning analysis of the membrane domain of CTR-copper transporters. *J. Membr. Biol.* 2010; **234**: 113–123.
31 Lemmon MA, Flanagan JM, Hunt JF, Adair BD, Bormann BJ, Dempsey CE, Engelman DM. Glycophorin A dimerization is driven by specific interactions between transmembrane alpha-helices. *J. Biol. Chem.* 1992; **267**: 7683–7689.
32 Li E, You M, Hristova K. Sodium dodecyl sulfate-polyacrylamide gel electrophoresis and Förster resonance energy transfer suggest weak interactions between fibroblast growth factor receptor 3 (FGFR3) transmembrane domains in the absence of extracellular domains and ligands. *Biochemistry* 2005; **44**: 352–360.

